

1 **Enhancing Reactant Selectivity for Ni/Mg Reforming Catalysts Using**
2 **Silicalite-1 Shells: A Modeling Study**

3 Brian Gray ^a, John N. Kuhn ^{a,*}, Babu Joseph ^a

4 a. University of South Florida, 4202 E Fowler Ave, Tampa, FL 33620

5 briancgray@usf.edu (B. Gray)

6 jnkuhn@usf.edu (J. Kuhn)

7 bjoseph@usf.edu (B. Joseph)

8 *Corresponding Author

9

10

11

12

13

14

15

16

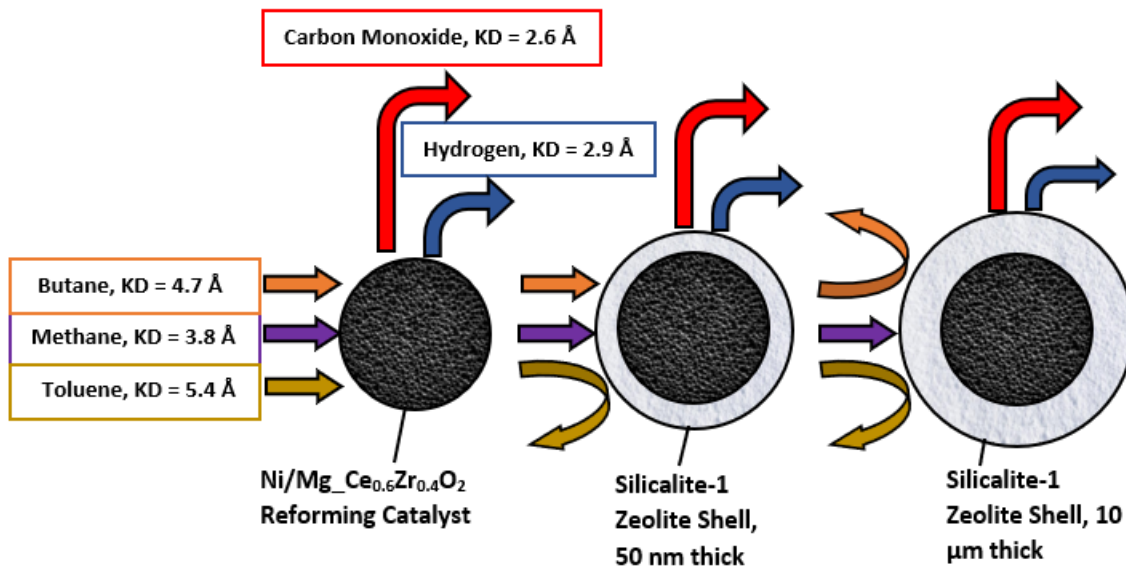
17

18 **Abstract**

19 The ability of a zeolite shell to enhance the selective conversion of hydrocarbons through diffusional
20 limitations was investigated using a multi-scale model of a fixed-bed reactor. The impact of shell thickness
21 and molecule/pore size on the catalytic performance of silicalite-1 zeolite encapsulated nickel catalyst
22 pellets for steam reforming of C1-C7 hydrocarbons is reported. A reaction-diffusion model using kinetic
23 expressions established in literature was employed. The model was verified through comparison with
24 reported experimental results for steam reforming data over a temperature range of 748 – 1113 K and
25 pressure of 1 – 10 bar. Comparisons are also made against experimental data for steam reforming in the
26 presence of a zeolite shell. Evaluation of the Weisz-Prater criterion for both the core and encapsulated
27 catalyst confirmed mass transfer limitation induced by the utilization of a zeolite shell. The model was
28 used to suggest an optimal thickness that balances diffusional limitations imposed by the zeolite layer on
29 methane versus that of the heavier hydrocarbons. The optimum thickness varied as a function of
30 hydrocarbon size and shape which determined the diffusion rates. For toluene and heptane, a 50 nm thick
31 shell was sufficient to wholly prevent reaction. Hydrocarbons like propane and butane required a shell 7.5
32 and 5 μm thick. Increasing the gas-hourly-space-velocity from 10,000 to 60,000 h^{-1} caused a decrease in
33 the optimum shell thickness. This approach can be modified for application to other mixed hydrocarbon
34 systems to predict optimal catalyst design.

35

36 **Graphical Abstract**



37

38

39 **Highlights**

- 40 • Zeolite shell can be used to control reactant selectivity
- 41 • Silicalite-1 shell caused diffusion limitations that vary with hydrocarbon size
- 42 • A 50nm thick shell sufficient to wholly prevent reforming of heptane and toluene
- 43 • Optimum shell thickness established for hydrocarbons depending on GHSV

44

45 **Keywords**

- 46 • Zeolites; diffusion (membrane); mass transfer; core-shell catalyst; optimization; steam reforming

47

48

49 **1.0 Introduction**

50 The study of microporous zeolites as catalyst shells has garnered significant attention in recent
51 years due to their ability to act as size and shape selective barriers[1-3]. Depending on the pore size
52 distribution of the zeolite, this selectivity can regulate the diffusion of reactants into a catalyst as well as
53 the diffusion of products out of a catalyst. This versatility in potential applications has given rise to
54 numerous studies regarding the use of zeolite encapsulated catalysts for a variety of reactions including
55 Fischer-Tropsch Synthesis (FTS), hydrocarbon reforming and hydrogenation[4-7]. Another critical feature
56 of zeolites is their ion-exchange capabilities which lend them a variable acidity. Consequently, zeolites are
57 widely used in a number of heterogeneous catalytic reaction systems as active catalysts. Studies have also
58 indicated that zeolites with an average pore diameter of less than 0.5 nm are associated with reduced
59 coke formation[8-10] with the assumed cause being the lack of necessary space for coke to effectively
60 form. As a result of these properties and developments in recent years, zeolites have become an emerging
61 technology in a number of reaction systems as both size-selective shells and tandem catalysts.

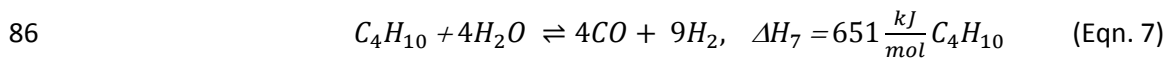
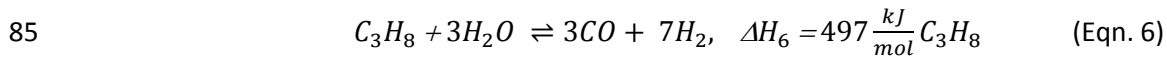
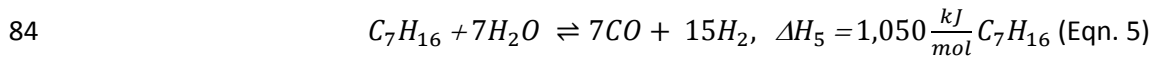
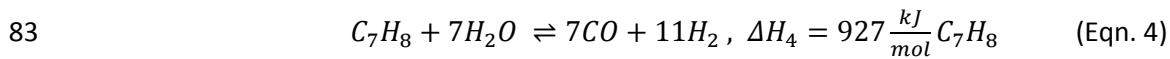
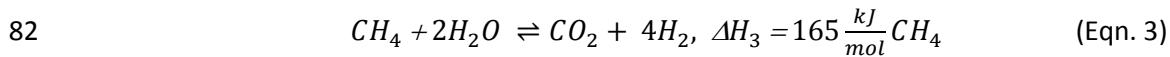
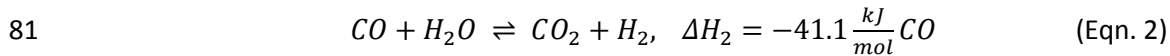
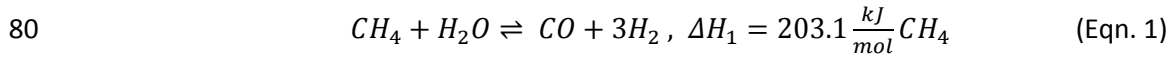
62
63 Herein, the application of a zeolite encapsulated catalyst is studied for application to the
64 production of syngas through hydrocarbon-steam reforming as part of a biomass to liquid (BTL) process.
65 The products of a biomass gasification reaction results in a stream composed of CO, CO₂, H₂, H₂O, CH₄ as
66 well as heavier hydrocarbons and contaminants [11]. The heavier hydrocarbons (referred to as tars for
67 aromatics) can significantly deactivate the reforming catalysts used in the syngas production step due to
68 coking [12]. The most common solution to this complication is the purification of the gas stream prior to
69 performing the reforming reaction. Complete purification is an expensive endeavor, and in the case of tar
70 removal, very difficult to achieve [13]. As a result, it becomes necessary to investigate methods by which
71 the reforming reaction can still be effectively performed even in the presence of tars. One such approach

72 is the introduction of a zeolite shell around the catalyst pellet to selectively reform the methane while
73 preventing the heavier hydrocarbons from reaching the catalyst.

74

75 In this study, toluene is used as a model tar component and the two terms will be used
76 interchangeably. Further, heptane, butane, and propane are included in the study to evaluate the effect
77 of molecular weight and kinetic diameter on the size selective properties of the zeolite. The principal
78 reactions for this steam reforming system are given below as eqns. 1-7:

79



87

88 Eqns. 1-3 describe standard temperature/pressure methane-steam reforming while 4 describes
89 toluene-steam reforming (TSR) [14, 15], Eqn. 5 describes heptane steam reforming (HSR) [16], Eqn. 6
90 applies to propane steam reforming (PSR)[17] and Eqn. 7 models steam reforming of butane (BSR)[18].
91 We investigate the application of a zeolite shell (pore diameter 0.5 nm) which acts as a size selective
92 barrier which prevents the toluene (kinetic diameter 0.585 nm) from accessing the inner reforming
93 catalyst. Methane (kinetic diameter 0.38 nm) however, can still pass through the zeolite pores to react.
94 Heptane was included in this study due to its similar molecular weight to toluene but smaller kinetic

95 diameter (0.43 nm). Propane and butane function as hydrocarbons intermediate to those above in terms
96 of molecular weight and kinetic diameter. The kinetic diameters and molecular weights of the studied
97 hydrocarbons are summarized in Table 1.

98

99 *Table 1: Comparison of molecular weight and kinetic diameter for hydrocarbon species*

Species	Molecular Weight (g/mol)	Kinetic Diameter (nm)
methane	16.04	0.38
propane	44.10	0.43
butane	58.12	0.47
toluene	92.14	0.54
heptane	100.21	0.43

100

101 The methane-toluene reforming system was experimentally investigated by Cimenler et al.[19]
102 who found that the inclusion of a zeolite shell was able to not only reduce the conversion of toluene, but
103 also enhance the conversion of methane in a combined reforming study. This was attributed to a
104 confinement effect between the core catalyst and zeolite shell. In the work of Zhang et al.[20] A relatively
105 thin shell of 3.5 μm was sufficient to protect a reforming catalyst from alkaline vapors without severe
106 hindrance of the methane. Due to the size of the zeolite pores, diffusion is typically considered to
107 transition from molecular to Knudsen diffusion[21]; however, studies have also indicated that, depending
108 on the zeolite and the diffusing species, a further transition into a configurational regime is also
109 possible[22, 23]. These observations present an optimization problem in which the beneficial effect of
110 increased selectivity toward lighter hydrocarbons and conversion of methane must be weighed against
111 the increased diffusional limitation introduced by the zeolite shell. These limitations result in reduced
112 reaction and overall conversion of reactants and may necessitate the use of a larger reactor to achieve a

113 specified conversion. Here, the use of a computational model incorporating reforming kinetics and species
114 diffusion through a composite catalyst to elucidate the optimum shell thickness for a silicalite-1 zeolite
115 shell on a 1.6 wt %Ni–1.2 wt % Mg/Ce_{0.6}Zr_{0.4}O₂ core catalyst is studied. The model is validated using
116 methane and toluene steam reforming data collected for a temperature range of 748 – 1113 K and
117 pressure from 1-10 bar in a fixed bed reactor. Later the model is used to evaluate the effect of the zeolite
118 shell thickness on reactant selectivity as a novel method by which the impact of a zeolite shell on the
119 diffusion of hydrocarbons of varying size may be studied. It is theorized that an optimum zeolite shell
120 thickness can be established which maximizes the relative conversion of methane over other hydrocarbon
121 species. This optimum value would also be dependent on the size and shape of the relevant hydrocarbons,
122 the associated kinetics, feed composition as well as the temperature, and pressure.

123 *1.1 Core-Shell Catalyst Experimental and Modeling Studies*

124 Cimenler et al.[24] undertook the experimental evaluation of the catalytic performance of a 51
125 wt% H-β zeolite, 1.6 wt %Ni–1.2 wt % Mg/Ce_{0.6}Zr_{0.4}O₂ core-shell catalyst for applications in MSR, TSR and
126 the combined steam reforming of methane and toluene. Cimenler found that the inclusion of a zeolite
127 shell introduced mass transfer limitations which reduced the conversion of hydrocarbons however the
128 reactant selectivity toward methane increased by a factor of 1.5. Furthermore, a weight hourly space
129 velocity (WHSV) comparison between the core-shell catalyst and a physical mixture of catalyst particles
130 and zeolite indicated that the H-β zeolite contributed to an increase in toluene conversion brought about
131 by its acidity or possible Al₃₊ promotion. An experimental and modeling study of MSR over Silicalite-1
132 encapsulated Ni/SiO₂ and Ni/Al₂O₃ catalysts was performed by Zhang et al. [20] with the objective of
133 reducing alkali-poisoning of catalysts in direct internal reforming molten carbonate fuel cells. To this end
134 the optimization of the shell thickness to maximize catalyst protection while minimizing loss in activity
135 due to diffusional limitation was performed. The inclusion of a zeolite shell was able to prevent catalyst

136 deactivation from electrolyte vapors expected under normal cell operating conditions, the optimum shell
137 thickness to achieve this effect balanced against minimizing diffusional limitations was 3.5 μm which
138 resulted in a $1/5^{\text{th}}$ decrease in methane conversion.

139 The experimental and modeling study on the size and shape selectivity of core-shell catalysts has also
140 been conducted for hydrogenation reactions by Kuo et al. [25] and Zhang et al. [26]. The work of Khan et
141 al. [27] successfully synthesized a microlayer of silicalite-1 zeolite on a Ni/SiO₂ core catalyst for use in the
142 hydrogenation of both the 1-hexene and 3,3-dimethyl-1-butene isomers. Khan noted, relative to the
143 core catalyst alone, the core-shell catalyst demonstrated excellent size selectivity with minimal decrease
144 in the conversion of 1-hexane. The system was also modeled for a simple packed bed reactor assuming
145 that the diffusion through the zeolite shell was the rate limiting step, the model was found to closely
146 agree with experimental data for space time from 0.25 – 1.5 (g*h/mol).

147

148 *1.2 Kinetic Modeling*

149 Modeling the kinetic behavior of hydrocarbon-steam reforming reactions is one that has seen
150 significant attention over the past decades. Numerous researchers have proposed rate laws ranging from
151 simple power laws to more complex Langmuir-Hinshelwood (LH) rate expressions and microkinetic
152 models [28-30]. There is no singular kinetic law that describes hydrocarbon reforming for all possible
153 catalysts and reaction conditions. Herein it was necessary to decide on rate expressions for the modeling
154 of the steam reforming of methane, toluene and a combined system containing both species.

155 Regarding methane steam reforming (MSR), one of the most established rate expressions is the
156 scheme put forth by Xu and Froment [31]. Utilizing a Nickel based catalyst on a magnesium spinel,
157 Froment's group had excellent agreement between modeled and experimental results for a temperature
158 range of 773 – 843 K and a steam to carbon (S/C) ratio of three and five. In the decades since its proposal

159 the reaction scheme has been successfully used for modeling MSR over Ni/Mg catalysts with minor
160 alterations to the rate parameters to fit catalysts with different metal loadings [32-34]. Sprung [29]
161 studied the effect of S/C ratio on the rate in a MSR process finding that as the S/C ratio decreases so too
162 does the order of reaction in the reaction scheme. It was concluded that, although generally accurate for
163 higher S/C ratios, the rate law proposed by Xu and Froment may not be applicable for applications with a
164 lower S/C ratio. Wei and Iglesia [30, 35] proposed an alternative mechanism finding through their
165 experimental works that the rates of reaction were proportional only with the partial pressure of methane
166 while being independent of other reactants; however, only a limited range of S/C variations were studied
167 and likely a factor in their findings. With these considerations in mind, it was decided to apply Xu and
168 Froment's rate expressions in this work utilizing rate parameters fit to experimental data using a least
169 squares approach. The rate expressions utilize a Langmuir-Hinshelwood mechanism (Eqns. 8-10). All three
170 rate equations [16-18] tend toward infinity as the partial pressure of hydrogen tends toward zero which
171 necessitates the inclusion of hydrogen in the gas feed though this was not found to strongly impact the
172 simulation of experimental results. This negative contribution to the rate is believed to be a result of the
173 method employed by Xu and Froment [31] for catalyst reduction wherein pure hydrogen was passed over
174 the catalyst for 12 hr. This combination of high concentration and time of exposure enhanced the
175 dissolution of hydrogen in the nickel resulting in increased hydrogen presence in the catalyst during
176 reaction [29].

177 Heptane steam reforming is modeled using the Langmuir-Hinshelwood mechanism proposed in
178 literature as in Eqn. 12[16]. Toluene and propane steam reforming have predominantly been modeled
179 using a straightforward first order power law in toluene and propane[17] respectively with great success
180 in simulating experimental results[14, 36, 37]. Steam reforming of butane has been successfully modeled
181 over Ni and Pt-Ni catalysts using a power law dependent on both butane and steam as noted in Eqn. 13.
182 Note that in this equation $\alpha=1.2$ and $\beta=-0.18$ [18].

$$r_1 = \frac{\frac{k_1}{p_{H_2}^{2.5}} \left(p_{CH_4} p_{H_2O} - \frac{p_{H_2}^3 p_{CO}}{K_1} \right)}{(DEN)^2}, \quad (\text{Eqn. 8})$$

$$r_2 = \frac{\frac{k_2}{p_{H_2}} \left(p_{CO} p_{H_2O} - \frac{p_{H_2}^3 p_{CO_2}}{K_2} \right)}{(DEN)^2}, \quad (\text{Eqn. 9})$$

$$r_3 = \frac{\frac{k_3}{p_{H_2}^{3.5}} \left(p_{CH_4} p_{H_2O}^2 - \frac{p_{H_2}^4 p_{CO_2}}{K_3} \right)}{(DEN)^2}, \quad (\text{Eqn. 10})$$

$$DEN = 1 + K_{CO} p_{CO} + K_{H_2} p_{H_2} + K_{CH_4} p_{CH_4} + \frac{K_{H_2O} p_{H_2O}}{p_{H_2}}, \quad (\text{Eqn. 11})$$

$$r_6 = \frac{\frac{k_6}{p_{H_2}^{2.5}} (p_{C_7H_{16}})}{\left(1 + \frac{0.2487 (p_{C_7H_{16}} p_{H_2})}{p_{H_2O}} + 0.077 \left(\frac{p_{H_2O}}{p_{H_2}} \right) \right)^2}, \quad (\text{Eqn. 12})$$

$$r_7 = k_7 (p_{C_4H_{10}})^\alpha (p_{H_2O})^\beta, \quad (\text{Eqn. 13})$$

189

190 2.0 Methodology

191 2.1 Model Overview

192 A stationary, isothermal multiscale model was designed which couples the bulk transport of
 193 species through the macroscale catalyst bed with the microscale transport through the catalyst pellet. The
 194 pressure drop was assumed to be negligible for the configurations considered. The bulk transport of
 195 species considers both convection and diffusional contributions and is modeled through solution of the
 196 one-dimensional version of Eqn. 14 in which $D_{m,i}$ is the molecular diffusivity of each species given through
 197 Eqn. 15. Boundary conditions of the macroscale ordinary differential equations (ODE's) are specified at
 198 the reactor inlet as the bulk concentration of the hydrocarbons, steam, and hydrogen and at the surface
 199 of the particle. It is assumed that the concentration at the particles surface is equal to the bulk
 200 concentration multiplied by the catalyst porosity. At the reactor outlet convection is assumed to dominate
 201 mass transport terms.

202
$$-D_{m,i} \frac{\partial^2 C_{i,x}}{\partial^2 x} - C_{i,x} U_x = R_i, \quad (\text{Eqn. 14})$$

203

204
$$D_{m,i} = \frac{10^{-3} T^{1.75} \left(\frac{1}{M_A} + \frac{1}{M_B} \right)^2}{P \left[(\Sigma V_A)^{\frac{1}{3}} + (\Sigma V_B)^{\frac{1}{3}} \right]^2}, \quad (\text{Eqn. 15})$$

205
$$R_i = (1 - \varepsilon) A_p \left(-D_{z,i} \frac{\partial C_{p,i}}{\partial r} \cdot \mathbf{n} \right), \quad (\text{Eqn. 16})$$

206 The reaction term R_i depends on the flux of each species at the boundary of the pellets. This flux
 207 is given in Eqn. 16. Proper solution of this reaction term requires the incorporation of a mass-balance for
 208 the interior catalyst pellets which acts as the microscale term. The dimensionless, mass transport equation
 209 for a spherical catalyst pellet is given in Eqn. 17 where $R_{p,i}$ refers to the rate of reaction within the catalyst
 210 pellet .

211
$$\nabla \cdot \left(- \left(\frac{r}{r_{\text{particle}}} \right)^2 D_{T,k} \frac{\partial C_{p,i}}{\partial r} \right) + \left(\frac{r}{r_{\text{particle}}} \right)^2 R_{p,i} = 0, \quad (\text{Eqn. 17})$$

212
$$D_{k,i} = 97 r_{\text{pore}} \left(\frac{T}{M_i} \right)^{1/2}, \quad (\text{Eqn. 18})$$

213
$$D_{C,i} = \frac{1}{z} \sqrt{\frac{8kT}{\pi M_i}} \gamma e^{-\frac{E_{C,i}}{R_g T}}, \quad (\text{Eqn. 19})$$

214
$$D_{ze}(T) = D_{ze}(T_r) \exp \left(-\frac{E_d}{R_g} \left(\frac{1}{T} - \frac{1}{T_r} \right) \right), \quad (\text{Eqn. 20})$$

215

216 Contribution to mass transport within the pellet interior are assumed to dominated by diffusion
 217 which is estimated as a combination of both the molecular and Knudsen diffusivities for
 218 $\text{CH}_4, \text{H}_2\text{O}, \text{H}_2, \text{CO}$ and CO_2 by Eqns. 15, 18. Studies have indicated that the diffusion of large molecules
 219 very near to the size of the zeolite pores such as toluene and heptane is strongly affected by molecule
 220 shape and size. This third diffusion regime, dubbed “configurational diffusion”, was used as a point of

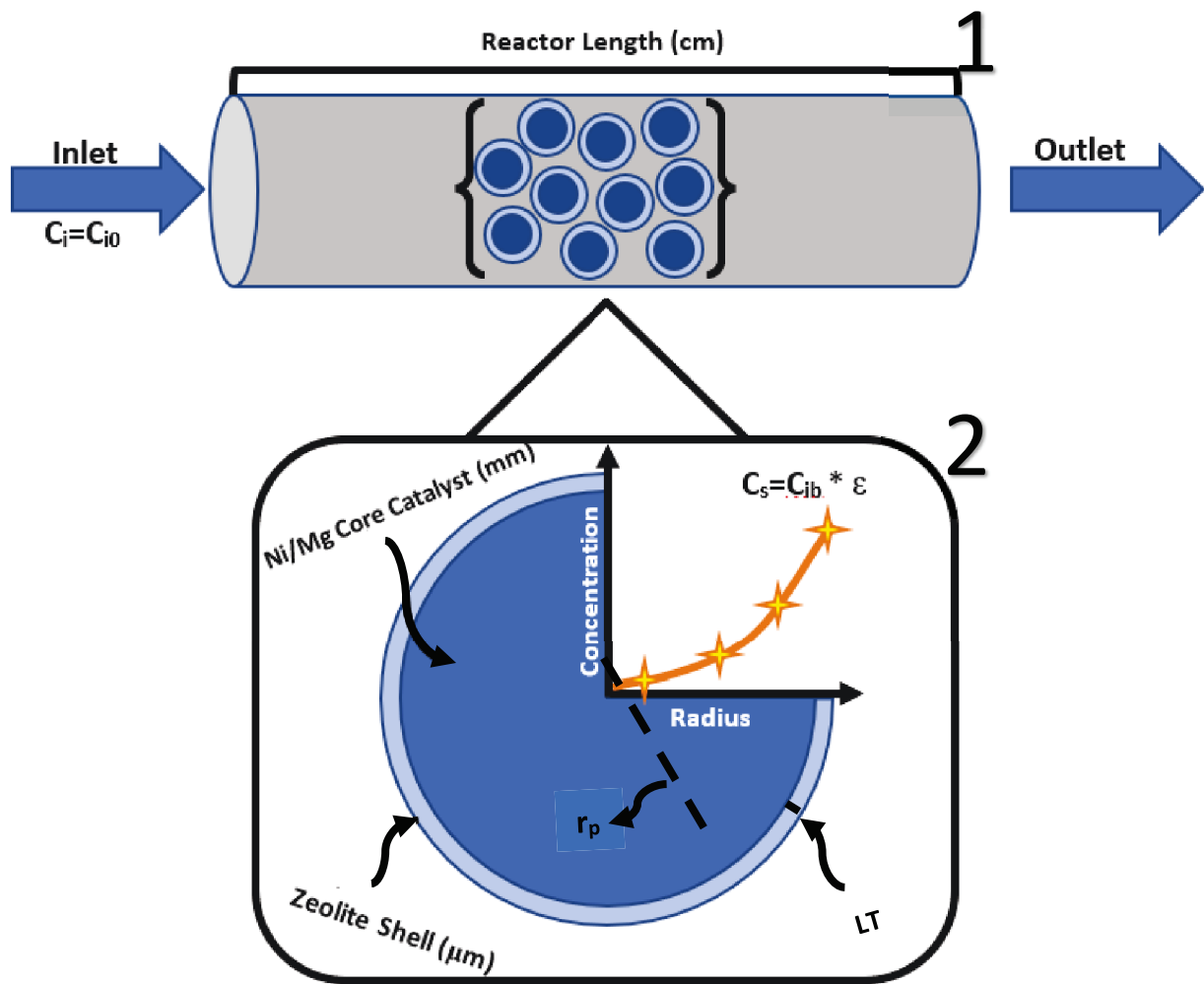
221 comparison for the diffusivity of toluene and heptane through the zeolite per Eqn. 19 where in the
 222 activation energy of diffusion was determined in accordance with the work of Xiao et al.[22]. The
 223 diffusivity coefficients used for the model are obtained from literature and adjusted to the reaction
 224 temperature using Eqn. 20. Due to a lack of agreement in estimations of diffusion through silicalite-1
 225 zeolite, correlations for Knudsen and configurational diffusion as defined in Eqns. 18 and 19 are used for
 226 comparison with the experimental terms to ensure accuracy of the estimate. Another important factor is
 227 the large temperature range over which the experimental results are interpolated (~300 to 1000K) as most
 228 studies are conducted at room temperature. Diffusivity terms are scaled according to the thickness of the
 229 pellet and zeolite shell respectively. For the core pellet, this scaling is given in Eqn. 21 while the diffusivity
 230 through the zeolite is modeled using Eqn. 22 wherein LT refers to the thickness of the zeolite shell and “r”
 231 is the pellet radius in which a value of zero points toward the pellet center and a value of one refers to
 232 the boundary of the catalyst pellet. Further, all diffusivities were estimated as effective diffusivities using
 233 typical values for tortuosity and porosity. Solution of the model differential equations is performed
 234 through the finite element method. For a full process diagram outlining the steps taken in development
 235 of the model and conduction of the study, see the Supporting Information, Appendix C.

236

Table 2: Boundary conditions for model scales

Scale	BC 1	BC 2
Macroscale Catalyst Bed	$C_{i_0} = C_{i_{in}} @ x = 0$	$\frac{dC_i}{dx} = 0 @ x = L$
Microscale Spherical Particle	$\frac{dC_i}{dr} = 0 @ r = 0$	$C_i = \varepsilon * C_{i_b} @ r = R$

237



238

239 *Figure 1: Graphic demonstrating basis of multiscale model design and associated length scales for the*
 240 *reactor, catalyst and zeolite shell. The first scale is a 1D bulk reactor with the second scale being a*
 241 *spherical catalyst pellet. “LT” refers to the thickness of the zeolite layer, “ r_p ” refers to the radius of the*
 242 *core catalyst.*

243

$$D_{T,1} = \frac{D_{p,i}}{r_{\text{particle}}^2 * r^2}, \quad (\text{Eqn. 21})$$

244

$$D_{T,2} = \frac{D_{z,i}}{LT^2 * (r-1)^2}, \quad (\text{Eqn. 22})$$

245

246

247

248

249 2.2 Parameter Estimation

250 Parameter estimation was carried out separately for the case of MSR and TSR to ensure the
251 accuracy of the chosen rate expressions for a broad selection of feed compositions, catalyst loadings,
252 temperatures, and pressures. For MSR, three rate constants and seven equilibrium constants were
253 present in the rate law. The temperature dependence of the rate constant and species-dependent
254 equilibrium constants were estimated using the Arrhenius and Van't Hoff equations respectively (eqns.
255 23,24). Overall equilibrium constants for each reaction were estimated using Eqns. 25-27. By contrast,
256 TSR, BSR and HSR, contained only the single overall rate parameter and the apparent activation energy
257 which needed to be considered.

$$258 \quad k_i = A_i \exp\left(-\frac{E}{RT}\right), \quad i = 1,2,3, \quad (\text{Eqn. 23})$$

$$259 \quad K_j = A_j \exp\left(-\frac{\Delta H}{RT}\right), \quad j = \text{CO, CH}_4, \text{H}_2\text{O, H}_2 \quad (\text{Eqn. 24})$$

$$260 \quad K_1 = 1.198E13 \exp\left(-\frac{26830}{T}\right), \quad (\text{Eqn. 25})$$

$$261 \quad K_2 = 1.767E - 2 \exp\left(-\frac{4400}{T}\right), \quad (\text{Eqn. 26})$$

$$262 \quad K_3 = 2.117E11 \exp\left(-\frac{22430}{T}\right), \quad (\text{Eqn. 27})$$

263 The fitting of the parameters to each data set was carried out through minimization of the sum of
264 the square of the error between experimental data and the model prediction for the overall conversion
265 of each respective hydrocarbon. The rate constants k_j were used for minimization following which the
266 activation energy and pre-exponential factor could be estimated using the resulting Arrhenius plots. The
267 list of reaction parameters considered in the fitting process as well as their final, fitted values can be
268 observed in Table 4. Fitting was performed for uncoated catalysts to ensure accuracy of kinetic rate

269 expressions in the case of absent mass transfer limitations. Tables 5 and 6 summarize the final reactor
 270 kinetic parameters used in the study. The reactor and catalyst are modeled after a typical 4 mm diameter,
 271 lab-scale, quartz reactor. The MSR kinetic parameters similar to those fit to the data from Zhang et al.
 272 were chosen as this is one of the few studies which experimentally evaluated the effect of the thickness
 273 of a zeolite shell on MSR. Validation of the estimation of diffusivities through typical catalyst pellets and
 274 zeolite shells was validated through comparison with experimental data collected for a defect-free,
 275 silicalite-1 zeolite encapsulated Ni/Al₂O₃ catalyst utilized for methane steam reforming for shell
 276 thicknesses between 0-100 μm. Validation of both the kinetic expressions as well as the estimated core-
 277 shell diffusivities enable the application of the model to determine the optimum zeolite shell thickness
 278 necessary to maximize the selectivity toward the lighter hydrocarbon over tars. The influence of the GHSV
 279 was also investigated. The resulting plots are given in Figure 2, in all cases agreement is observed between
 280 the model and experimental data indicating the suitability of the model for predicting MSR and TSR
 281 behavior.

282

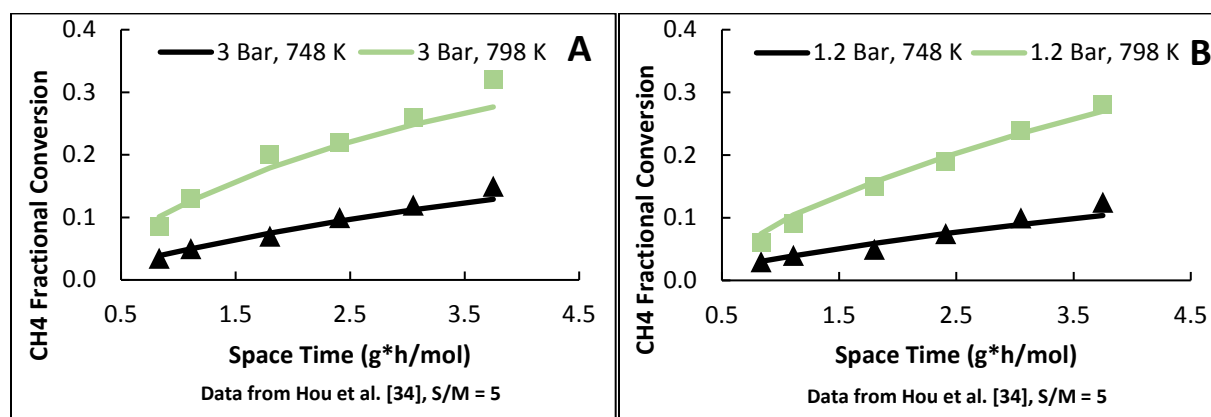
283 *Table 3: Collection of referenced reaction conditions using for model fitting and validation*

Reference	Temperature (K)	Pressure (bar)	Catalyst	Loading (mg)	H ₂ O:CxHy
MSR					
[24]	1053-1113	1	1.6 wt % Ni 1.2 wt % Mg/Ce _{0.6} Zr _{0.4} O ₂	11.3	1:1
[38]	748, 798	1.2, 3	Ni/α-Al ₂ O ₃	100	5:1
TSR					
[24]	1053-1113	1	1.6 wt %	11.3	7:1

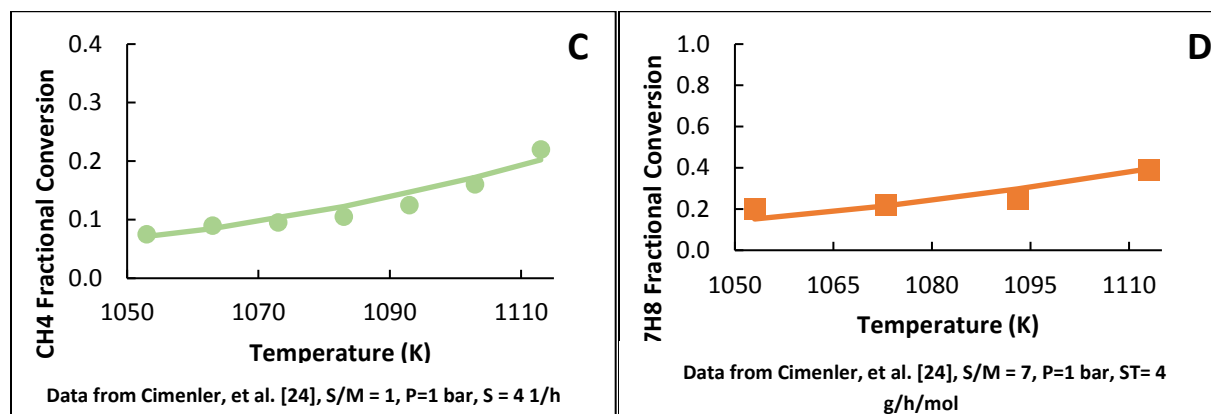
			Ni-1.2 wt % Mg/Ce _{0.6} Zr _{0.4} O ₂		
[14]	923, 1073	1	Ni/Olivine	5-300	7:1
Composite MSR					
[20]	923	1	Ni/Al ₂ O ₃ -Sil-1	800	3:1

284

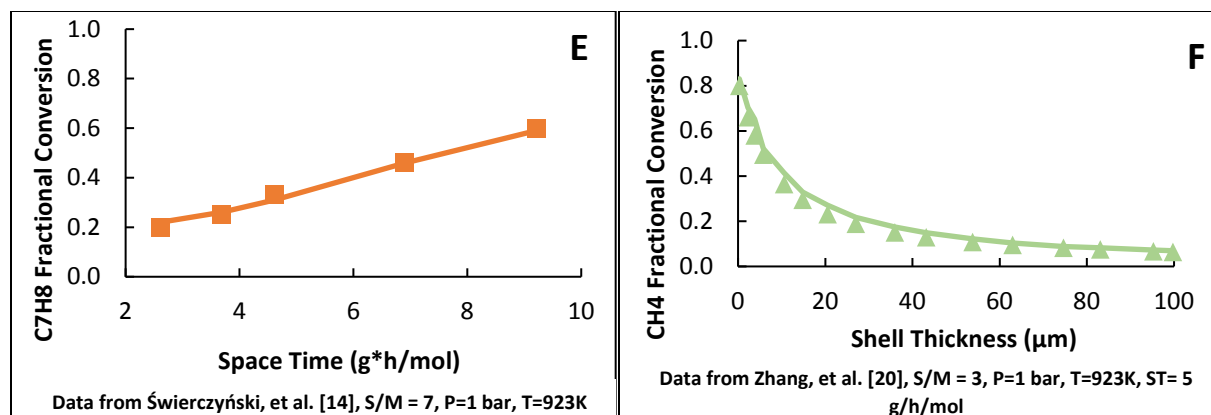
285



286



287



288

289 Figure 2: Comparison between model (lines) and experimental data (Points) for (A) MSR vs space time
 290 from the work of Hou, et al[38]. for T=748, 798 K and P=3 bar. (B) MSR vs space time from the work of
 291 Hou, et al[38]. for T=748, 798 K and P=1.2 bar. (C) MSR vs temperature from the work of Cimenler, et
 292 al[24]. (D) TSR vs temperature from work of Cimenler, et al[24]. (E) TSR vs space time from work of
 293 Świerczyński, et al.[14] and (F) MSR vs zeolite shell thickness from the work of Zhang, et al[20].

294

295 Table 4: Fitted kinetic parameters for modeling of referenced experimental data

Parameter	Fitted Values				
	Ref. 24 (MSR)	Ref. 35 (MSR)	Ref. 14 (TSR)	Ref. 24 (TSR)	Ref. 20 (MSR)
A_1	1.63E+16	4.02E+20	-	-	4.22E+15
A_2	1.00E+03	1.75E-04	-	-	1.955E+6
A_3	1.00E+15	1.40E+09	-	-	1.020E+15
A_4	-	-	3.13E+13	2.74E+12	
E_1	348	295	-	-	240
E_2	59	68.1	-	-	67
E_3	354	144	-	-	243
E_4	-	-	196	197.8	

296

297

298 *2.3 Study Metrics and Parameters*

299 Model performance was evaluated through study of hydrocarbon conversions, Eqn. 28, in
300 addition to the surface rate of reaction at the entrance of the reactor for both hydrocarbons. Initially, a
301 kinetics only study is performed for an uncoated catalyst. The effects of the S/C ratio, pressure and
302 reaction temperature on hydrocarbon conversions are evaluated to determine optimum operating
303 conditions to maximize selective conversion of methane. Following this, the effect of the zeolite shell
304 thickness is evaluated for the chosen operating conditions.

305

$$306 \quad X_i = \frac{F_{i0} - F_i}{F_{i0}}, \quad (\text{Eqn. 28})$$

307

308 Following model validation, reaction parameters were selected to mimic benchtop reaction
309 studies and to ensure kinetics did not reach equilibrium. The initial modeling studies focus on an
310 unencapsulated reforming catalyst with model parameters as given in Table 3. The model was explored
311 for a temperature range of 800-1000 K, pressure from 1-10 bar and a steam to methane (S/M) ratio of 2,
312 4, 6, 8 and 10 to evaluate the response of methane and toluene activity to the tested conditions. In this
313 manner, optimum conditions to maximize the activity of methane relative to toluene were established.
314 The ratio of species in the feed is given as 1:0.1:0.1 methane: toluene: hydrogen. The flow of argon is
315 adjusted to maintain a constant gas hourly space velocity (GHSV). Following this, the effect of zeolite shell
316 thickness was studied at the determined optimum operating conditions obtained through study of the
317 unencapsulated model. At these conditions pore diffusion limitations, identified through evaluation of the
318 Weisz-Prater (W-P) criterion, were not present for the unencapsulated catalyst, see supporting
319 information for corresponding calculations. The kinetic parameters used in the model correspond to those

320 obtained through fitting to the data referenced from Zhang et al. This particular reference was chosen as
321 it is one of the few works which utilize a Silicalite-1 zeolite shell for MSR.

322

323 *Table 5: Final model reactor parameters and feed conditions for the model*

Symbol	Study 1	Unit
L	25E-3	m
r_r	2E-3	m
M_{Cat}	0.5	g
r_p	0.3E-3	m
χ_{CH_4}	0.25	-
χ_{H_2O}	0.709	-
$\chi_{C_7H_8}$	0.01	-
$\chi_{C_7H_{16}}$	0.01	-
$\chi_{C_3H_8}$	0.01	-
$\chi_{C_4H_{10}}$	0.01	-
χ_{H_2}	0.001	-

324

325

326 *Table 6: Final model kinetic parameters*

Symbol	Value	Unit
A_1	4.22E15	$\frac{mol}{kg\ s}$
A_2	1.95E06	$\frac{m\ s\ mol}{kg^2}$

A_3	1.02E15	$\frac{mol}{kg\ s}$
A_4	4.83E08	$\frac{m^3}{kg\ s}$
A_5	8.00E03	$\frac{m\ s\ mol}{kg^2}$
A_6	2.00E08	$\frac{m^3}{kg\ s}$
A_7	1.83E06	$\frac{mol}{bar\ kg\ s}$
A_{CO}	8.23E-5	1/bar
A_{H_2}	6.12E-9	1/bar
A_{CH_4}	6.65E-4	1/bar
A_{H_2O}	1.77E5	-
E_1	267	kJ/mol
E_2	67.13	kJ/mol
E_3	260	kJ/mol
$E_{C_7H_8}$	190	kJ/mol
$E_{C_7H_{16}}$	110	kJ/mol
$E_{C_3H_8}$	95	kJ/mol

327

328 To evaluate the point at which the balance between the diffusion limitations imposed on the other
329 hydrocarbons relative to methane is at a maximum, an objective function (OF) was proposed. The
330 proposed OF functions as a quantitative measure of the effect of the thickness of the zeolite shell on the
331 conversion of each hydrocarbon. It is defined as the difference between the change in the conversion as
332 a function of shell thickness, for each hydrocarbon and that of methane. This difference is then normalized

333 by the rate of change in methane conversion as a function of shell thickness, Eqn. 29. The use of this
 334 objective function allows the evaluation of the rate of change in the conversion as a function of shell
 335 thickness for each hydrocarbon relative to that of methane for a shell thickness of 0-50 μm .

336

337
$$OF = \frac{\frac{dX_{CH_4}}{dLT} - \frac{dX_i}{dLT}}{\frac{dX_{CH_4}}{dLT}}, i = C_3H_8, C_4H_{10}, C_7H_8, C_7H_{16}, \text{ (Eqn. 29)}$$

338

339 *Table 7: Diffusion coefficient through zeolite layer as obtained from literature and estimated using*

340 *Knudsen and configurational diffusivity correlations*

Species	D_{ze} , Experimental* (m^2/s)	D_{ze} , Knudsen** (m^2/s)	D_{ze} , Configurational*** (m^2/s)
CH ₄	7.70E-08	1.92E-07	1.34E-09
C ₃ H ₈	5.02E-09	1.16E-07	1.34E-10
C ₄ H ₁₀	1.89E-09	1.00E-07	3.20E-11
C ₇ H ₈	8.16E-13	7.99E-08	8.78E-13
C ₇ H ₁₆	9.35E-12	7.59E-08	4.74E-12

341 *Diffusion coefficient obtained from literature and adjusted to 1000K using Eqn. 14 and parameters from Table 8

342 **Determined through Eqn. 12

343 ***Determined through Eqn. 13

344

345 *Table 8: Parameters used to determine diffusion of hydrocarbons through Silicalite-1 zeolite*

Species	$D_{ze}(T_r)$ [Reference] (m^2/s)	T_r (K)	$E_{d,i}$ [Reference] (kJ/mol)
CH ₄	1.60E-08[39]	300	5.6[39]
C ₃ H ₈	1.20E-09[39]	300	5.1[39]

C_4H_{10}	2.00E-10[39]	300	8[39]
C_7H_8	2.00E-16[40]	283	22[40]
C_7H_{16}	1.30E-14[41]	323	18.8[42]

346

347 Table 7 summarizes the diffusion coefficients of each hydrocarbon species obtained from
348 literature or estimated using Knudsen and configurational diffusion correlations. Notably, the
349 Experimental diffusion coefficients for methane and propane are relatively close to those predicted by
350 Eqn. 12. Considering the small kinetic diameters of these molecules, configuration diffusion does not
351 appear to be applicable. By contrast, butane does not seem to be accurately modeled by either Knudsen
352 or configurational diffusion indicating that this species likely falls into a “transitional” regime.
353 Consequently, the experimental value was used for this species in the model. Both toluene and heptane
354 observe very good agreement between literature values and those predicted by Eqn. 13. From this it is
355 interpreted that these larger hydrocarbons will experience severe diffusion limitations in the zeolite shell
356 owing to their large molecular size. The work of Maginn et al.[43] simulates the diffusion of n-alkanes in
357 silicalite ranging from carbon number 1 – 20. Results for lighter alkanes with carbon number 1-4 have
358 close agreement with experimental data however for moderate and long chain alkanes the predicted
359 values diverge from some values reported in literature. Thus, this work was referenced for the diffusion
360 of methane, propane and butane while the works of Kolsch et al.[41] and Cartarius et al.[40] were cited
361 for the study of heptane and toluene respectively.

362 To justify the assumption of isothermal operation, the Anderson and Mears criterion for intra and
363 interphase heat transfer was calculated. Both in the absence and presence of a zeolite shell the estimated
364 criterion was several orders of magnitude below the limit at which heat transfer gradients become
365 apparent. This result supports the decision to assume the isothermal condition. The full calculations can
366 be found in the Supporting Information, Appendix B. Likewise the Weisz-Prater criterion for pore and bulk

367 diffusion was estimated in Appendix B. Mass transfer limitations were not present for any hydrocarbon
368 for the uncoated catalyst. Upon introduction of the zeolite shell all hydrocarbons exhibited diffusion
369 limitations which varied by the size of each hydrocarbon.

370

371 **3.0 Results and Discussion**

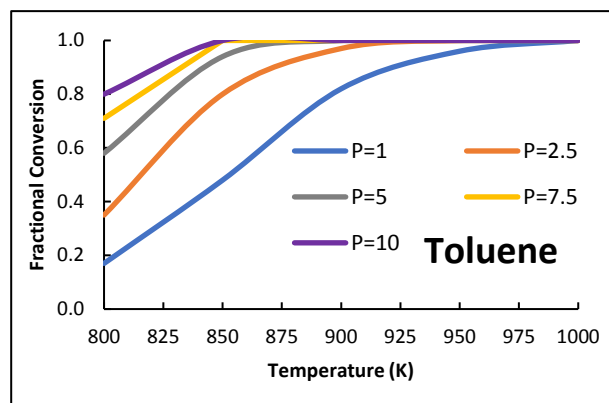
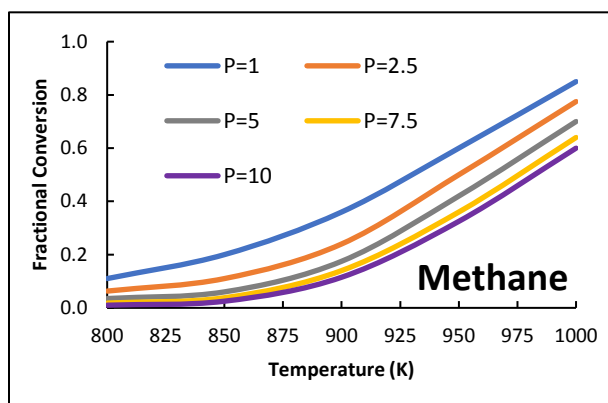
372 *3.1 Zeolite Characterization*

373 Considering the relative diameters of the zeolite pores and the toluene molecules, it seems
374 apparent that tars would be unable to diffuse through the shell pores. However, both experimental and
375 modeling efforts indicate the reaction of toluene. It is generally held in literature that Silicalite-1 zeolite
376 does not contribute to hydrocarbon reforming, thus tar molecules must be diffusing through the zeolite
377 shell. The micropore size distribution of Silicalite-1 is characteristically narrow and averages a width of 0.5
378 nm. There are, however, pores which are slightly larger than this average value. Considering the relative
379 nearness of the kinetic diameter of toluene (0.54 nm) to the average micropore width (0.5 nm), it seems
380 plausible that some toluene molecules may diffuse through pores which fall on the higher end of the
381 distribution. Silicalite-1 also contains a small minority of mesopores which could likewise facilitate
382 diffusion. A second explanation is the presence of cracks and pinholes in the zeolite shell. The work of
383 Cimenler et. al. indicated the presence of such cracks, identified through scanning electron micrographs,
384 averaging 5.26 microns in width on the zeolite shell. The structure of zeolites is also susceptible to
385 degradation at high temperature and in the presence of steam as is the case for this study in a process
386 commonly referred to as “steaming”. The presence of such defects could facilitate tar diffusion, thus
387 explaining the observed reaction of toluene.

388

389 *3.2 Screening Results*

390 Initial study of the modeled system in the absence of a zeolite shell allowed verification of the
391 optimum reaction conditions at which CH₄ reactivity is enhanced opposed to toluene. Toluene activity is
392 enhanced as the total pressure is increased. By contrast, methane reforming is well known to be
393 suppressed with increasing pressure. This behavior is in accordance with past studies on the reforming of
394 heavy hydrocarbons. Reaction of both hydrocarbons is predictably enhanced with increasing
395 temperature; however, toluene is generally more active than methane at all temperatures. Little change
396 is observed for changing the S/M ratio likely because excess steam is flowed through the reactor and the
397 catalyst is already saturated with water molecules. From this initial study, the reaction conditions for the
398 zeolite studies were selected as T=1000 K, P=1bar and S/M=2.8



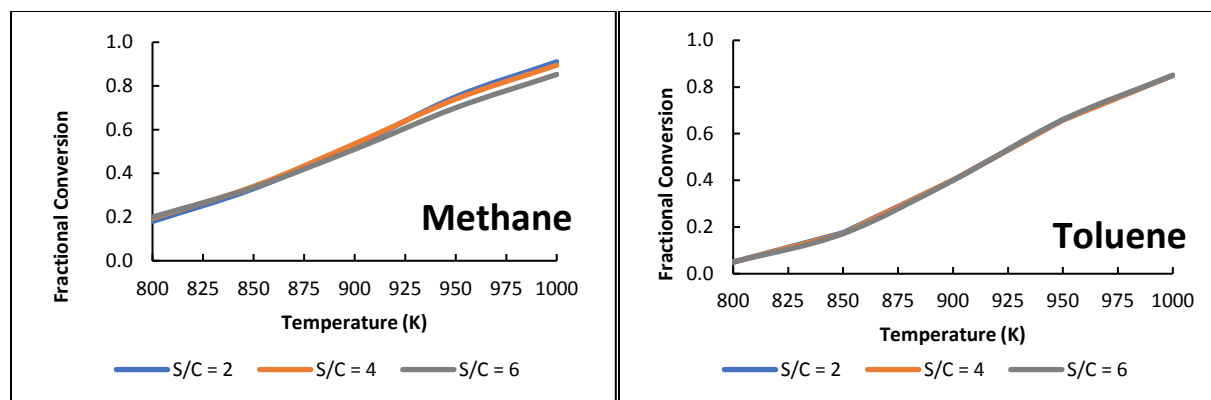
399

400

401

402

403



404
 405 *Figure 3: (Top) Conversion of methane and Toluene against temperature for a pressure of 1, 2.5, 5, 7.5*
 406 *and 10 bar, S/C=1. (Bottom) Conversion of methane and Toluene against temperature for S/C ratio of 2,*
 407 *4 and 6, P=1 bar.*

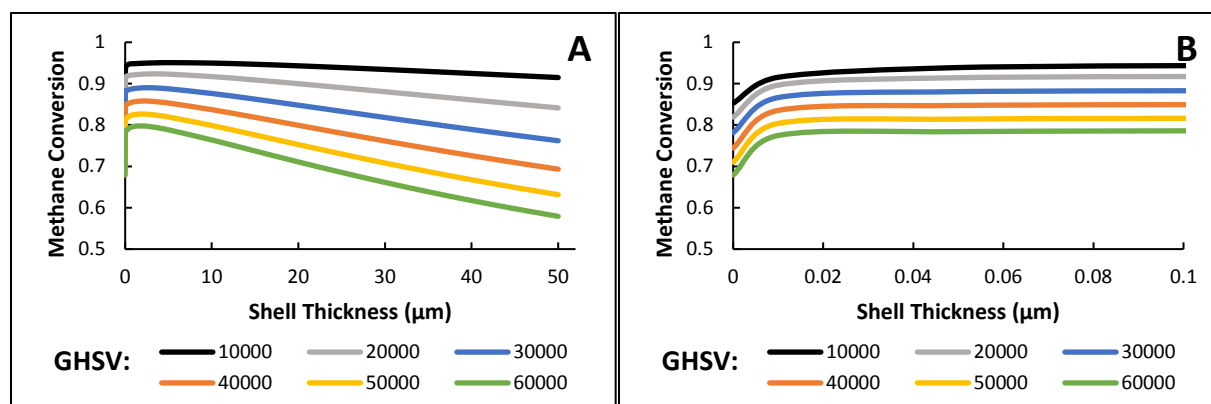
408

409 3.3 Investigation of Zeolite Shell

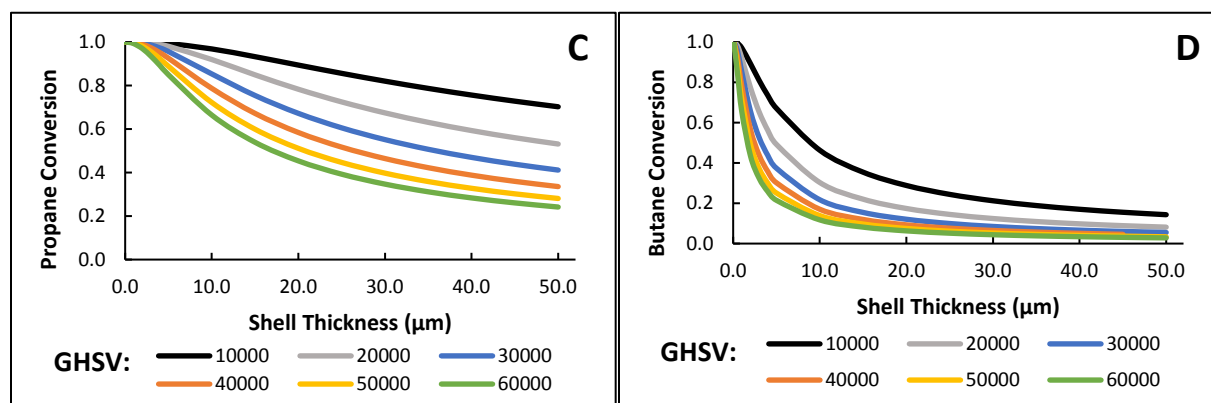
410 Evaluation of the influence of the zeolite shell on the five hydrocarbons is captured in Figure 4. It
 411 is generally noted that both toluene and heptane exhibit severe loss in reactivity with the introduction of
 412 relatively thin zeolite shell (10-1000 nm). Toluene in particular appears to be severely impeded by the
 413 inclusion of a zeolite shell of nearly any thickness. Heptane also observes a significant reduction in reaction
 414 with the inclusion of a thin shell on the order of a few nanometers. For a shell merely 10 nm thick and a
 415 GHSV of $10,000 \frac{1}{h}$, toluene conversion was reduced from 100% to 17% and heptane reduced from a
 416 likewise complete conversion to 72%. At these same conditions, both butane and propane remained
 417 unhindered at near complete conversion. It is noted that methane in fact observes an apparent
 418 enhancement in activity at low zeolite shell thicknesses (50 nm-10 μm). This is likely due to changes in
 419 equilibrium brought about by the severe reduction in conversion in the heavier hydrocarbons. The
 420 thermodynamic equilibrium conversion of methane both with and without the presence of the heavier
 421 hydrocarbons is plotted in Figure A.1 in Appendix A under the Supporting Information. In the absence of
 422 other hydrocarbons, the equilibrium conversion of methane increases from 87% to 98%. It is likely that

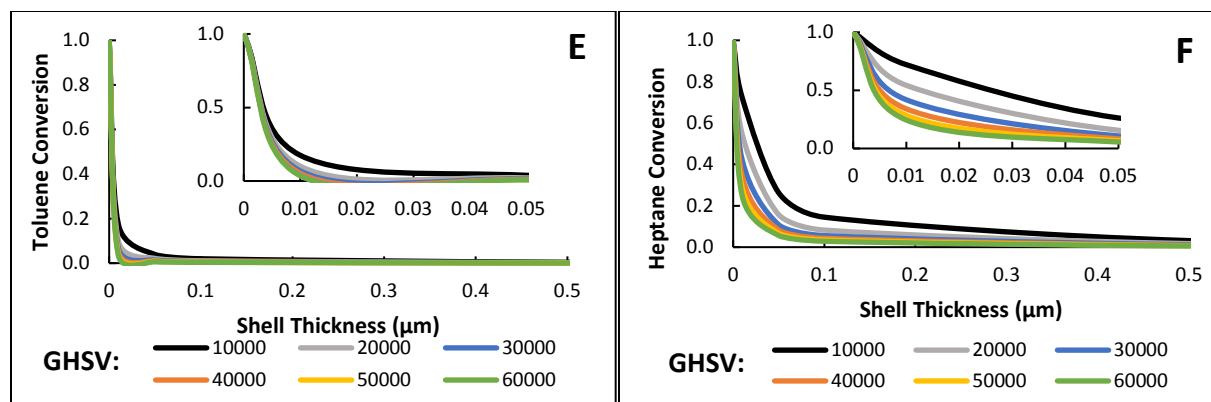
423 the complete conversion of the heavy hydrocarbons results in significantly more syngas production which
424 pushes the equilibrium conversion of methane to lower values. With the introduction of a zeolite shell,
425 the larger hydrocarbons are effectively impeded and thus unable to react, the result of which is an
426 increase in equilibrium conversion of methane. As the zeolite thickness increases further however
427 methane begins to be impeded and more diffusion limitations are introduced. It is noted however that
428 even at a GHSV of $60,000 \frac{1}{h}$ and a $50 \mu\text{m}$ thick shell methane conversion is only reduced to 60% while
429 propane is reduced to 24% and toluene, heptane, and butane are unable to react nearly entirely.

430



432





433

434 *Figure 4: Conversion of (A) methane, (B) zoomed in methane plot, (C) propane, (D) butane, (E) heptane*
 435 *and (F) toluene against zeolite shell thickness for varying GHSV, $T=1000K$, $P=1bar$, $S/M = 2.8$*

436

437 Through application of the objective function as defined in section 2.5, the optimum zeolite shell
 438 thickness for each hydrocarbon species relative to methane was obtained. When plotted as a function of
 439 effective diffusivity (Figure 5), the system behaves as expected. As the diffusion coefficient of the species
 440 becomes larger, a correspondingly thicker shell is necessary to significantly hinder reaction of a
 441 hydrocarbon species. This effect appears to be fairly linear at larger diffusivity coefficients on the order of
 442 $1E-9 m^2/s$. As the coefficient approaches the order of $1E-12 m^2/s$ further reduction in the diffusivity no
 443 longer has a notable effect on the optimum shell thickness as a zeolite shell of any thickness can effectively
 444 block the hydrocarbon. At low GHSV, the effect is slightly exponential

445

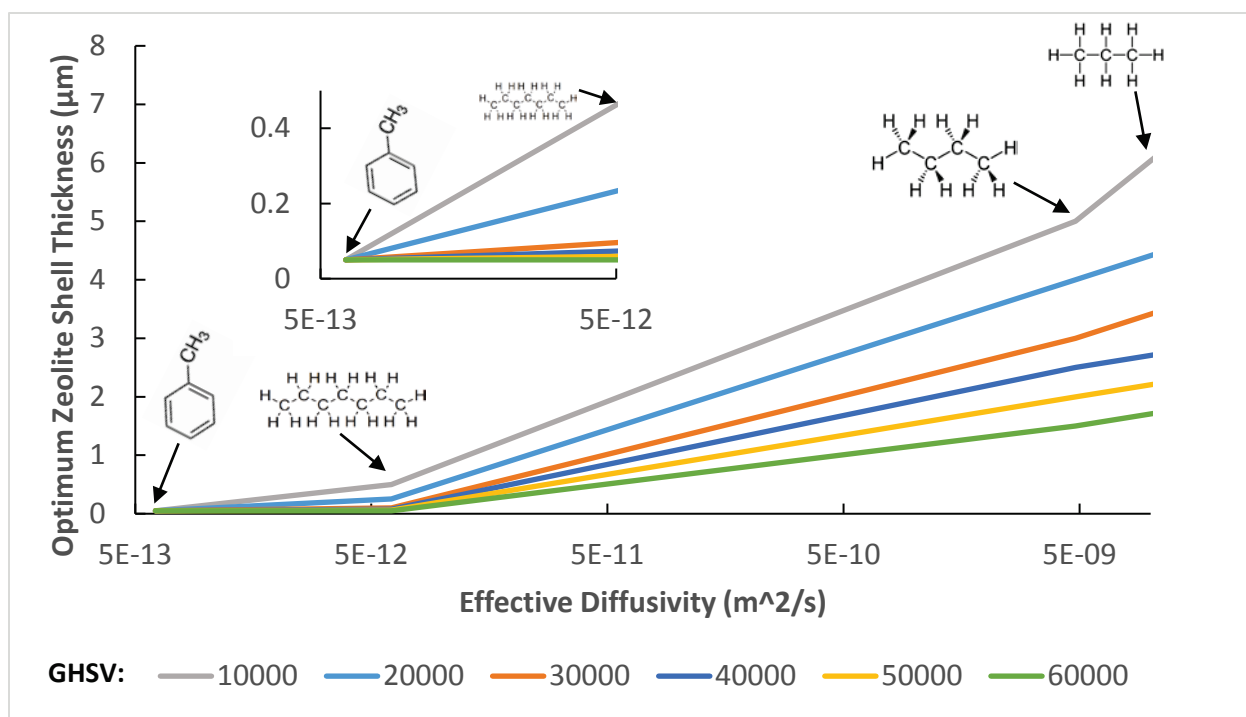
446 Efforts were made to plot this optimum as a function of molecular weight and kinetic diameter
 447 however these efforts indicated that both of these parameters must be considered to properly compare
 448 aromatics and moderate chain alkanes. The kinetic diameter, which is one parameter used in the
 449 estimation of diffusivity through the configurational diffusivity correlations, is reported as 4.3 \AA for
 450 alkanes with carbon numbers from three to ten. For an aromatic such as toluene, this is reported as 5.4
 451 \AA . This would imply that the performance of heptane would be similar to species such as propane in terms

452 of diffusivity. In actuality however, the diffusion coefficient of heptane is closer to that of toluene and the
453 resulting plot shows discontinuities at a kinetic diameter of 4.3 Å.

454
455 Discontinuities likewise became apparent when the optimum shell thickness was plotted as a
456 function of molecular weight. In this case these discontinuities are a result of heptane having a slightly
457 larger molecular weight than toluene while also having a larger coefficient of diffusion. This deviation in
458 diffusivity arises from differences in shape of each species. Both toluene and heptane are in the
459 configurational regime of diffusion as observed by comparisons to modeled and experimental data in
460 Table 7. In this regime the size and shape of the molecule dominates the estimation of diffusivity. While
461 toluene is nearly uniform in all dimensions, there is a significant difference between the minimum and
462 maximum diameters of the heptane molecule. This raises the vital question of how diffusivity of species
463 should be modeled. Performance of each hydrocarbon species is highly dependent on the respective
464 diffusion coefficient through the zeolite and as a result, accurate estimation of the parameter is essential.
465 Conventional methods would indicate that for the diffusion of species through a zeolite pore, Knudsen
466 diffusivity would dominate. Knudsen diffusion, however, has no dependence on the size of a molecule;
467 only its molecular weight. It is clear however when comparing the experimental diffusion coefficients of
468 heptane and toluene through zeolites as well as the modeling results demonstrated here that this is
469 insufficient. It is then clear that both kinetic diameter and molecular weight must be considered to
470 properly compare the effect of a zeolite shell on a mix of alkanes and aromatic species. It is for this reason
471 that the effective diffusivity, which incorporates both, was used as the point of comparison.

472
473 The optimum shell thickness for a given species is defined relative to methane. For heavier and
474 larger species, such as aromatics and long chain hydrocarbons, a relatively thin zeolite shell is sufficient
475 to prevent significant reaction without overtly hindering the diffusion of lighter species such as methane.

476 In some instances, the zeolite shell can even result in enhancement of reactant activity due to shifts in
 477 equilibrium. GHSV was also observed to influence the optimum shell thickness, this is likely a result of the
 478 definition of the OF, specifically how it is normalized by the performance of methane. An increase in GHSV
 479 reduces the conversion of all species while increasing the rate of reaction. As the least active hydrocarbon
 480 in the system, methane exhibits the largest loss in performance with increasing GHSV in the absence of a
 481 zeolite shell. Even for a low GHSV of 10,000, it only takes a shell merely 50nm in thickness to wholly
 482 prevent the reaction of toluene and heptane. Regarding the lighter hydrocarbons, propane and butane,
 483 at a GHSV of 10,000 the predicted optimum shell thickness for these species was 7.5 and 5 μm
 484 respectively. At these thicknesses, the conversion of butane was reduced to 67%. Propane conversion was
 485 still approximately 96% at the predicted optimum shell thickness. This is likely a result of the similarity
 486 between propane and methane in terms of diffusivity and the definition of "optimum shell thickness".
 487 Even though propane is not significantly hindered, methane conversion has been enhanced by nearly 10%.
 488



489

490

491 *Figure 5: Determined optimum zeolite shell thickness as a function of effective diffusivity for varying*

492 $GHSV \left(\frac{1}{h}\right)$

493 **4.0 Conclusion**

494 The multiscale model developed showed close agreement to experimental data. The zeolite shell
495 inhibited the diffusion of all hydrocarbons; however, the larger hydrocarbons were much more strongly
496 affected as expected. A criterion was developed to determine the optimal thickness to balance diffusional
497 limitations imposed by the zeolite shell on desired and undesired reactions. The optimal thickness is a
498 strong function of the effective diffusivity of the hydrocarbon taking into account the size and shape
499 features. The kinetic diameter and molecular weight both affect the diffusivity which in turn determines
500 the optimum shell thickness desired for that molecule. The effect of diffusivity on the optimum shell
501 thickness was approximately linear up to a value on the order of E-12 at which point further decreases in
502 diffusivity did not yield any significant impact on the shell thickness. When molecular weight was used as
503 the basis of comparison, it seems apparent that heptane is both the heavier and larger hydrocarbon.
504 However, when comparing model results and reported diffusion coefficient in literature, it is observed
505 that heptane diffuses slightly more readily in zeolite. This behavior is best explained by the effect of the
506 orientation of a molecule on its ability to diffuse through a pore. While toluene is a more rigid and
507 symmetric aromatic hydrocarbon, a more flexible, moderate-chain hydrocarbon can diffuse more readily
508 at specific orientations. For toluene and heptane, a 10 nm thick shell was sufficient to wholly inhibit
509 reaction through induced mass transfer limitations. Hydrocarbons like propane and butane required a
510 shell 7.5 and 5 μm thick. Increasing the gas-hourly-space-velocity from 10,000 to 60,000 h^{-1} caused a
511 decrease in the optimum shell thickness.

512

513 **Acknowledgement**

514 This research was supported by the US Department of Energy (DOE) under award DE- EE0008488.

515 **Declaration of Interests**

516 Dr. Babu Joseph, and Dr. John Kuhn disclose an interest in patents on related subjects issued to University
517 of South Florida.

518 This report was prepared as an account of work sponsored by an agency of the US government.
519 Neither the US government nor any agency thereof, nor any of their employees, makes any warranty,
520 express or implied, or assumes any legal liability or responsibility for the accuracy, completeness, or
521 usefulness of any information, apparatus, product, or process disclosed, or represents that its use would
522 not infringe on privately owned rights. Reference herein to any specific commercial product, process, or
523 service by trade name, trademark, manufacturer, or otherwise does not necessarily constitute or imply
524 its endorsement, recommendation, or favoring by the US government or any agency thereof. The views
525 and opinions of authors expressed herein do not necessarily state or reflect those of the US government
526 or any agency thereof.

527 **Notation**

α	Power law dependence of n-butane in butane steam reforming	-
β	Power law dependence of steam in butane steam reforming	-
ϵ	Porosity of catalyst bed	-
γ	Distance between adjacent sites	-
A_j	Preexponential factor for rate constants k_j	-
A_i	Preexponential factor for constants K_i	-
A_p	Surface to volume ratio of catalyst particle	
C_i	Concentration of species "i"	mol m ⁻³
C_{ib}	Bulk concentration of species "i"	mol m ⁻³

$C_{s,i}$	Concentration of species "i" at the catalyst particle surface	mol m^{-3}
$C_{p,i}$	Concentration of species "i" within the catalyst particle	mol m^{-3}
$D_{m,i}$	Molecular diffusivity of species "i" <i>in steam</i>	$\text{m}^2 \text{s}^{-1}$
$D_{k,i}$	Knudsen diffusivity of species "i"	$\text{m}^2 \text{s}^{-1}$
$D_{C,i}$	Configurational diffusivity of species "i"	$\text{m}^2 \text{s}^{-1}$
$D_{e,i}$	Effective diffusivity of species "i"	$\text{m}^2 \text{s}^{-1}$
$D_{p,i}$	Diffusivity of species "i" through core catalyst	$\text{m}^2 \text{s}^{-1}$
$D_{z,i}$	Diffusivity of species "i" through zeolite shell	$\text{m}^2 \text{s}^{-1}$
$D_{T,k}$	Scaled diffusion through model scale "k"	-
E_j	Activation energy for reaction "j"	kJ mol^{-1}
$E_{d,i}$	Activation energy of diffusion for species "i"	kJ mol^{-1}
$E_{c,i}$	Activation energy of configurational diffusion for species "i"	kJ mol^{-1}
F_{i0}	Inlet molar flow of species "i"	mol hr^{-1}
F_i	Molar flow of species "i"	mol hr^{-1}
$K_{1,3}$	Equilibrium constant for steam reforming reactions 1 and 3	bar^2
K_2	Equilibrium constant for steam reforming reaction 2	-
K_i	Adsorption constant for species "i"	-
k_j	Rate constant for reaction "j"	-
k	Boltzmanns constant	$\text{m}^2 \text{kg s}^{-2} \text{K}^{-1}$
ΔH_j	Enthalpy of reaction for reaction "j"	kJ mol^{-1}
L	Length of reaction zone	m
LT	Thickness of zeolite shell	m
M_i	Molar mass of species "i"	g mol^{-1}
M_{Cat}	Mass of catalyst	g
N	Interparticle flux vector	$\text{mol m}^{-2} \text{s}^{-1}$
n	Outward flux vector	$\text{mol m}^{-2} \text{s}^{-1}$

p_{i0}	Partial pressure of species "i"	bar
P	Total pressure	bar
r_r	Radius of reactor	m
$r_{particle}$	Radius of core catalyst	m
r_{pore}	Radius of core catalyst pores	m
r_j	Rate of reaction of reaction "j"	$\text{mol g}^{-1} \text{hr}^{-1}$
$R_{p,i}$	Interparticle rate of reaction for species "i"	$\text{mol g}^{-1} \text{hr}^{-1}$
R_g	Gas constant	$\text{J mol}^{-1} \text{K}^{-1}$
T	Temperature	K
T_0	Reference temperature for diffusivity coefficients in table 8	K
T_r	Reference temperature used for parameter estimation	K
u	Flow velocity	m s^{-1}
V_i	Atomic diffusion volume	m^3
X_i	Conversion of species "i"	-
χ_i	Mole Fraction of species "i"	-
z	Coordination number	-

528

529

530 Works Cited

- 531 [1] K. Cheng, J. Kang, S. Huang, Z. You, Q. Zhang, J. Ding, W. Hua, Y. Lou, W. Deng, Y. Wang, Mesoporous
532 Beta Zeolite-Supported Ruthenium Nanoparticles for Selective Conversion of Synthesis Gas to C5–C11
533 Isoparaffins, *Acs Catal*, 2 (2012) 441-449 DOI: 10.1021/cs200670j.
- 534 [2] M. Niwa, N. Katada, K. Okumura, Characterization and design of zeolite catalysts: solid acidity, shape
535 selectivity and loading properties, Springer Science & Business Media, 2010.
- 536 [3] M. Okamoto, Core–Shell Structured Zeolite Catalysts with Minimal Defects for Improvement of Shape
537 Selectivity, in: *Core-Shell and Yolk-Shell Nanocatalysts*, Springer, 2021, pp. 187-198.

538 [4] C.H. Kuo, Y. Tang, L.Y. Chou, B.T. Sneed, C.N. Brodsky, Z.P. Zhao, C.K. Tsung, Yolk-Shell
539 Nanocrystal@ZIF-8 Nanostructures for Gas-Phase Heterogeneous Catalysis with Selectivity Control, *J Am*
540 *Chem Soc*, 134 (2012) 14345-14348 DOI: 10.1021/ja306869j.

541 [5] W.N. Zhang, G. Lu, C.L. Cui, Y.Y. Liu, S.Z. Li, W.J. Yan, C. Xing, Y.R. Chi, Y.H. Yang, F.W. Huo, A Family of
542 Metal-Organic Frameworks Exhibiting Size-Selective Catalysis with Encapsulated Noble-Metal
543 Nanoparticles, *Adv Mater*, 26 (2014) 4056-4060 DOI: 10.1002/adma.201400620.

544 [6] E.A. Khan, A. Rajendran, Z.P. Lai, Synthesis of Ni-SiO₂/Silicalite-1 Core-Shell Micromembrane Reactors
545 and Their Reaction/Diffusion Performance, *Ind Eng Chem Res*, 49 (2010) 12423-12428 DOI:
546 10.1021/ie101850j.

547 [7] S.A. Gardezi, B. Joseph, Performance Characteristics of Eggshell Co/SiO₂ Fischer-Tropsch Catalysts: A
548 Modeling Study, *Ind Eng Chem Res*, 54 (2015) 8080-8092 DOI: 10.1021/acs.iecr.5b01288.

549 [8] J. Jae, G.A. Tompsett, A.J. Foster, K.D. Hammond, S.M. Auerbach, R.F. Lobo, G.W. Huber, Investigation
550 into the shape selectivity of zeolite catalysts for biomass conversion, *J Catal*, 279 (2011) 257-268 DOI:
551 10.1016/j.jcat.2011.01.019.

552 [9] H. Karge, Coke formation on zeolites, in: *Stud Surf Sci Catal*, Elsevier, 1991, pp. 531-570.

553 [10] K. Lee, S. Lee, Y. Jun, M. Choi, Cooperative effects of zeolite mesoporosity and defect sites on the
554 amount and location of coke formation and its consequence in deactivation, *J Catal*, 347 (2017) 222-230
555 DOI: 10.1016/j.jcat.2017.01.018.

556 [11] M. Kılıç, A.E. Pütün, B.B. Uzun, E. Pütün, Converting of oil shale and biomass into liquid hydrocarbons
557 via pyrolysis, *Energ Convers Manage*, 78 (2014) 461-467 DOI: 10.1016/j.enconman.2013.11.002.

558 [12] P. Simell, Effects of gasification gas components on tar and ammonia decomposition over hot gas
559 cleanup catalysts, *Fuel*, 76 (1997) 1117-1127 DOI: 10.1016/s0016-2361(97)00109-9.

560 [13] P. Hasler, T. Nussbaumer, Gas cleaning for IC engine applications from fixed bed biomass gasification,
561 *Biomass and Bioenergy*, 16 (1999) 385-395 DOI: 10.1016/s0961-9534(99)00018-5.

562 [14] D. Swierczynski, C. Courson, A. Kiennemann, Study of steam reforming of toluene used as model
563 compound of tar produced by biomass gasification, *Chemical Engineering and Processing: Process*
564 *Intensification*, 47 (2008) 508-513 DOI: 10.1016/j.cep.2007.01.012.

565 [15] B. Zhao, X. Zhang, L. Chen, R. Qu, G. Meng, X. Yi, L. Sun, Steam reforming of toluene as model
566 compound of biomass pyrolysis tar for hydrogen, *Biomass and Bioenergy*, 34 (2010) 140-144 DOI:
567 10.1016/j.biombioe.2009.10.011.

568 [16] M.E.E. Abashar, Steam reforming of n-heptane for production of hydrogen and syngas, *Int J Hydrogen*
569 *Energ*, 38 (2013) 861-869 DOI: 10.1016/j.ijhydene.2012.10.081.

570

571 [17] S.I. Uskov, L.V. Enikeeva, D.I. Potemkin, V.D. Belyaev, P.V. Snytnikov, I.M. Gubaidullin, V.A. Kirillov,
572 V.A. Sobyenin, Kinetics of low-temperature steam reforming of propane in a methane excess on a Ni-
573 based catalyst, *Catal Ind*, 9 (2017) 104-109 DOI: 10.1134/s2070050417020118.

574 [18] A.K. Avci, D.L. Trimm, A.E. Aksoylu, Z.I. Onsan, Hydrogen production by steam reforming of n-butane
575 over supported Ni and Pt-Ni catalysts, *Appl Catal a-Gen*, 258 (2004) 235-240 DOI:
576 10.1016/j.apcata.2003.016.

- 577 [19] U. Cimenler, B. Joseph, J.N. Kuhn, Hydrocarbon steam reforming using Silicalite-1 zeolite
578 encapsulated Ni-based catalyst, *Aiche J*, 63 (2017) 200-207 DOI: 10.1002/aic.15521.
- 579 [20] J. Zhang, X. Zhang, M. Tu, W. Liu, H. Liu, J. Qiu, L. Zhou, Z. Shao, H.L. Ho, K.L. Yeung, Preparation of
580 core (Ni base)–shell (Silicalite-1) catalysts and their application for alkali resistance in direct internal
581 reforming molten carbonate fuel cell, *J Power Sources*, 198 (2012) 14-22 DOI:
582 10.1016/j.jpowsour.2011.09.070.
- 583 [21] V. Novák, P. Kočí, M. Marek, F. Štěpánek, P. Blanco-García, G. Jones, Multi-scale modelling and
584 measurements of diffusion through porous catalytic coatings: An application to exhaust gas oxidation,
585 *Catal Today*, 188 (2012) 62-69 DOI: 10.1016/j.cattod.2012.03.049.
- 586 [22] J. Xiao, J. Wei, Diffusion mechanism of hydrocarbons in zeolites—I. Theory, *Chem Eng Sci*, 47 (1992)
587 1123-1141 DOI: 10.1016/0009-2509(92)80236-6.
- 588 [23] W.O. Haag, R.M. Lago, P.B. Weisz, Transport and reactivity of hydrocarbon molecules in a shape-
589 selective zeolite, *Faraday Discussions of the Chemical Society*, 72 (1981) 317-330 DOI:
590 10.1039/dc9817200317.
- 591 [24] U. Cimenler, B. Joseph, J.N. Kuhn, Effect of Zeolite Membrane Shell Thickness on Reactant Selectivity
592 for Hydrocarbon Steam Reforming Using Layered Catalysts, *Energ Fuel*, 30 (2016) 5300-5308 DOI:
593 10.1021/acs.energyfuels.6b00510.
- 594 [25] C.H. Kuo, Y. Tang, L.Y. Chou, B.T. Sneed, C.N. Brodsky, Z. Zhao, C.K. Tsung, Yolk-shell nanocrystal@ZIF-
595 8 nanostructures for gas-phase heterogeneous catalysis with selectivity control, *J Am Chem Soc*, 134
596 (2012) 14345-14348 DOI: 10.1021/ja306869j.
- 597 [26] W. Zhang, G. Lu, C. Cui, Y. Liu, S. Li, W. Yan, C. Xing, Y.R. Chi, Y. Yang, F. Huo, A family of metal-organic
598 frameworks exhibiting size-selective catalysis with encapsulated noble-metal nanoparticles, *Adv Mater*,
599 26 (2014) 4056-4060 DOI: 10.1002/adma.201400620.
- 600 [27] E.A. Khan, A. Rajendran, Z. Lai, Synthesis of Ni–SiO₂/Silicalite-1 Core–Shell Micromembrane Reactors
601 and Their Reaction/Diffusion Performance, *Ind Eng Chem Res*, 49 (2010) 12423-12428 DOI:
602 10.1021/ie101850j.
- 603 [28] J.R. Rostrup-Nielsen, J. Sehested, J.K. Norskov, Hydrogen and synthesis gas by steam- and CO₂
604 reforming, *Adv Catal*, 47 (2002) 65-139 DOI: Doi 10.1016/S0360-0564(02)47006-X.
- 605 [29] C. Sprung, B. Arstad, U. Olsbye, Methane Steam Reforming over a Ni/NiAl₂O₄ Model Catalyst-Kinetics,
606 *Chemcatchem*, 6 (2014) 1969-1982 DOI: 10.1002/cctc.201402017.
- 607 [30] J. Wei, E. Iglesia, Isotopic and kinetic assessment of the mechanism of methane reforming and
608 decomposition reactions on supported iridium catalysts, *Phys Chem Chem Phys*, 6 (2004) 3754-3759 DOI:
609 10.1039/b400934g.
- 610 [31] J. Xu, G.F. Froment, Methane steam reforming, methanation and water-gas shift: I. Intrinsic kinetics,
611 *Aiche J*, 35 (1989) 88-96 DOI: 10.1002/aic.690350109.
- 612 [32] A. Alipour-Dehkordi, M.H. Khademi, O₂, H₂O or CO₂ side-feeding policy in methane tri-reforming
613 reactor: The role of influencing parameters, *Int J Hydrogen Energ*, 45 (2020) 15239-15253 DOI:
614 10.1016/j.ijhydene.2020.03.239.

615 [33] A. Iulianelli, G. Manzolini, M. De Falco, S. Campanari, T. Longo, S. Liguori, A. Basile, H₂ production by
616 low pressure methane steam reforming in a Pd–Ag membrane reactor over a Ni-based catalyst:
617 Experimental and modeling, *Int J Hydrogen Energ*, 35 (2010) 11514-11524 DOI:
618 10.1016/j.ijhydene.2010.06.049.

619 [34] M. Khzouz, E.I. Gkanas, Experimental and Numerical Study of Low Temperature Methane Steam
620 Reforming for Hydrogen Production, *Catalysts*, 8 (2017) DOI: 10.3390/catal8010005.

621 [35] J. Wei, E. Iglesia, Isotopic and kinetic assessment of the mechanism of reactions of CH₄ with CO₂ or
622 H₂O to form synthesis gas and carbon on nickel catalysts, *J Catal*, 224 (2004) 370-383 DOI:
623 10.1016/j.jcat.2004.02.032.

624 [36] C. Li, D. Hirabayashi, K. Suzuki, Development of new nickel based catalyst for biomass tar steam
625 reforming producing H₂-rich syngas, *Fuel Process Technol*, 90 (2009) 790-796 DOI:
626 10.1016/j.fuproc.2009.02.007.

627 [37] G. Oh, S.Y. Park, M.W. Seo, Y.K. Kim, H.W. Ra, J.-G. Lee, S.J. Yoon, Ni/Ru–Mn/Al₂O₃ catalysts for
628 steam reforming of toluene as model biomass tar, *Renew Energ*, 86 (2016) 841-847 DOI:
629 10.1016/j.renene.2015.09.013.

630 [38] K. Hou, R. Hughes, The kinetics of methane steam reforming over a Ni/ α -Al₂O₃ catalyst, *Chem Eng J*,
631 82 (2001) 311-328 DOI: 10.1016/s1385-8947(00)00367-3.

632 [39] E.J. Maginn, A.T. Bell, D.N. Theodorou, Dynamics of long n-alkanes in silicalite: A hierarchical
633 simulation approach, *J Phys Chem-Us*, 100 (1996) 7155-7173 DOI: DOI 10.1021/jp953200j.

634 [40] R. Cartarius, H. Vogel, J. Dembowski, Investigation of sorption and intracrystalline diffusion of
635 benzene and toluene on silicalite-1, *Ber Bunsen Phys Chem*, 101 (1997) 193-199 DOI: DOI
636 10.1002/bbpc.19971010206.

637 [41] P. Kolsch, D. Venzke, M. Noack, E. Lieske, P. Toussaint, J. Caro, Preparation and Testing of Silicalite-
638 in-Metal-Membranes, *Stud Surf Sci Catal*, 84 (1994) 1075-1082.

639 [42] O. Talu, M.S. Sun, D.B. Shah, Diffusivities of n-alkanes in silicalite by steady-state single-crystal
640 membrane technique, *Aiche J*, 44 (1998) 681-694 DOI: 10.1002/aic.690440316.

641 [43] E.J. Maginn, A.T. Bell, D.N. Theodorou, Dynamics of Long n-Alkanes in Silicalite: A Hierarchical
642 Simulation Approach, *The Journal of Physical Chemistry*, 100 (1996) 7155-7173 DOI: 10.1021/jp953200j.

643

644